Lithium Ion Batteries

Deutsche Ausgabe: DOI: 10.1002/ange.201509083
Internationale Ausgabe: DOI: 10.1002/anie.201509083

Li_2C_2, a High-Capacity Cathode Material for Lithium Ion Batteries

Na Tian[+], Yurui Gao[+], Yurong Li, Zhaoxiang Wang, Xiaoyan Song, and Liquan Chen*

Abstract: *As a typical alkaline earth metal carbide, lithium carbide (Li_2C_2) has the highest theoretical specific capacity (1400 mA h g^{-1}) among all the reported lithium-containing cathode materials for lithium ion batteries. Herein, the feasibility of using Li_2C_2 as a cathode material was studied. The results show that at least half of the lithium can be extracted from Li_2C_2 and the reversible specific capacity reaches 700 mA h g^{-1}. The C≡C bond tends to rotate to form C4 (C≡C···C≡C) chains during lithium extraction, as indicated with the first-principles molecular dynamics (FPMD) simulation. The low electronic and ionic conductivity are believed to be responsible for the potential gap between charge and discharge, as is supported with density functional theory (DFT) calculations and Arrhenius fitting results. These findings illustrate the feasibility to use the alkali and alkaline earth metal carbides as high-capacity electrode materials for secondary batteries.*

Lithium ion batteries (LIBs) are finding more and more important applications in electric vehicles and electricity storage stations after the great success in various portable electronic devices and tools. The conventional cathode materials that have only half the available capacity (mostly below 200 mA h g^{-1}) of the graphitic anodes (over 350 mA h g^{-1}) are becoming the bottleneck to the increase of energy density of the LIBs. Among all the reported lithium transition metal oxide cathode materials, the manganese-based lithium-rich layer-structured oxides, $x\,Li_2MnO_3\cdot(1-x)LiMO_2$ (M = Ni, Co, Mn), are expected to deliver a specific capacity over 250 mA h g^{-1}. However, quick decay of the capacity and discharge voltage,[1,2] severe O_2 evolution,[3] and poor rate performance[4] hinder their commercialization. Similar to the lithium-rich cathode materials, the layered $LiNi_{1-x-y}Co_xMn_yO_2$ (viable capacity below 200 mA h g^{-1}) cannot be applied in energy storage systems before their safety and cycling issues are properly addressed, especially when charged to high potentials (above 4.55 V vs. Li^+/Li).

Except for the inorganic cathode materials such as oxides, phosphides, and silicates, electroactive organics or polymers such as $Li_2C_6O_6$,[5] $Li_2C_8H_4O_4$,[6] and the Prussian blue catalogs[7] have also been studied as promising candidates of electrode materials. In contrast to the inorganic electrode materials that store or convert energy by valence changes of the transition-metal or the anions (such as O^{2-}), the organic electrode materials store Li ions by changing the charge state of the electroactive organic groups or moieties, for example, C=O. The advantages of the organic electrode lie in their higher theoretical capacity, safety, sustainability, environmental friendliness and potentially low cost. However, their cycling and rate performances are usually poor owing to the dissolution in the electrolyte and the low electric conductivity of the organic electrode materials.[5,6,8]

A number of Li-C binary carbides have been reported. For example, LiC_6, LiC_{12}, and LiC_{18} are well known products of lithium intercalation into graphite.[9] Li_4C_3 and Li_4C_5[10,11] were also reported and known as poly-lithium organic compounds. However, all these carbides are thermodynamically metastable; they are decomposed to Li_2C_2 at enhanced temperatures.[11,12]

Lithium carbide (Li_2C_2) was firstly prepared by Moissan et al.[13] in an electric furnace in 1896, with coal and Li_2CO_3 as the precursor. Its structure was determined to be orthorhombic in 1965.[14] Based on refinement to the powder X-ray diffraction (XRD) patterns, the distance between two nearest C atoms was determined to be 120 pm,[14] in good agreement with the bond length of the C≡C triple bond.[15] Figure 1a shows the unit cell of Li_2C_2 (space group Immm), with all of the C atoms in the same plane while all of the Li atoms are in another plane (Figure 1a).

[*] N. Tian,[+] Dr. Y. Gao,[+] Prof.Dr. Z. Wang, Prof.Dr. L. Chen
Key Laboratory for Renewable Energy
Chinese Academy of Sciences
Beijing Key Laboratory for New Energy Materials and Devices
Beijing National Laboratory for Condense Matter Physics
Institute of Physics, Chinese Academy of Sciences
P. O. Box 603, Beijing 100190 (China)
E-mail: zxwang@iphy.ac.cn
Y. Li, Prof.Dr. X. Song
College of Materials Science and Engineering
Key Laboratory of Advanced Functional Materials
Ministry of Education of China
Beijing University of Technology
Beijing 100124 (China)
[+] These authors contributed equally to this work.

Supporting information for this article is available on the WWW under http://dx.doi.org/10.1002/anie.201509083.

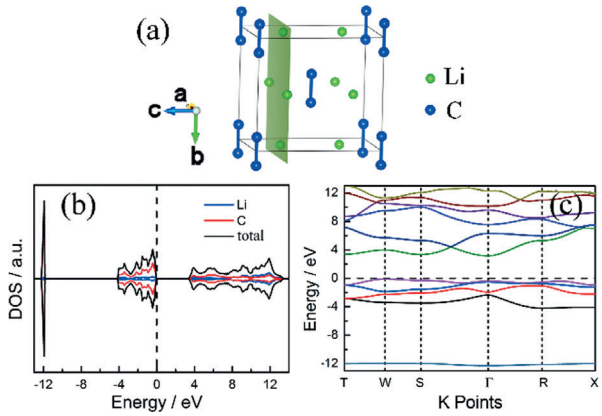

Figure 1. The unit cell (a), total and local density of states (DOS; b) and the spin-up band structure (c) of orthorhombic Li_2C_2.

Li_2C_2 is no stranger to the field of LIBs, although no one has ever attempted to use it as an electrode material. Schmitz et al.[16] claimed its presence in the solid electrolyte interphase (SEI) layer on a lithium-plated copper electrode, although it has not been experimentally observed. Recently, we found that Li_2C_2 can be obtained as a reduction product of Li_2CO_3 that is electrochemically converted from $CoCO_3$. It can react with the metallic cobalt to form Li_2CO_3 and finally $CoCO_3$ as the cell is recharged to 3.0 V versus Li^+/Li.[17] However, the properties of Li_2C_2 as a cathode material have never been studied. Nor is Li_2C_2 alone in the carbide family. There are a number of alkali metal carbides (Na_2C_2 (PDF No. 76-1713), K_2C_2 (No.76-1714)) and alkaline earth metal carbides (BeC_2 (No.33-0191), MgC_2 (No.03-0748), CaC_2 (No.82-0627)). These carbides are characteristic of their C≡C units. The partial breaking/recovering or distortion of the C≡C group makes them potential electrode materials in Li-, Na-, and Mg-ion batteries. They store Li-, Na-, and Mg-ions by changing the charge state of their C≡C groups.

Herein, we report the electrochemical performances of orthorhombic lithium carbide (Li_2C_2) and its structural evolution during cycling as a cathode material of lithium-ion batteries.

The electronic structure of Li_2C_2 was studied by density functional theory (DFT). Figure 1 b shows the local density of states (LDOS) of the atoms in Li_2C_2. The sharp DOS peaks at around −12 eV are actually the contribution of C2s-2p (sp1) hybridization, while the states near the Fermi level are dominantly that of C2p. As the spin-up and spin-down of the total DOS are completely symmetric, Li_2C_2 is a zero-magnetism material. Furthermore, the electronic structure (Figure 1 c) shows that the band gap of Li_2C_2 is 3.2 eV, with the bottom of the conduction band at the Γ-point and the top of the valence band at the W-point. As a result, the electronic conductivity of Li_2C_2 is expected to be low, and therefore it is essential to improve its electrical conductivity before any potential commercial application.

The average delithiation potential of Li_2C_2 is calculated to be 4.2 V when 0.5 Li/f.u. (f.u. for Li_2C_2 formula unit) is removed from the unit cell according to Equation (1). This indicates that Li_2C_2 might be used as a high-potential cathode material.

$$V_{\max}(x_1 \le x \le x_2) = -\frac{E_{Li_{2-x_1}C_2} - E_{Li_{2-x_2}C_2} - (x_2 - x_1)E_{Li}}{(x_2 - x_1)e} \quad (1)$$

Figure 2 a shows the XRD patterns of as-prepared Li_2C_2 powder before and after exposure to air (25 °C and 50 % RH) for 24 h. It is clear that the crystallinity of the as-prepared Li_2C_2 is low. The dominant phase of the material is orthorhombic Li_2C_2 (PDF No. 74-0268), though some impurity peaks (arrows marked) can be observed. The impurity phase is recognized to be metallic lithium (No. 01-1264), as a result of lithium excess in the precursor of Li_2C_2. A wide peak appears around 20° (2θ) after air exposure, indicating that part of the Li_2C_2 is decomposed to amorphous carbon. Therefore, Li_2C_2 is rather stable but cannot be stored in humid air for long. Figure 2 b shows the Raman spectrum of the as-prepared sample. The central position of the Raman spectrum

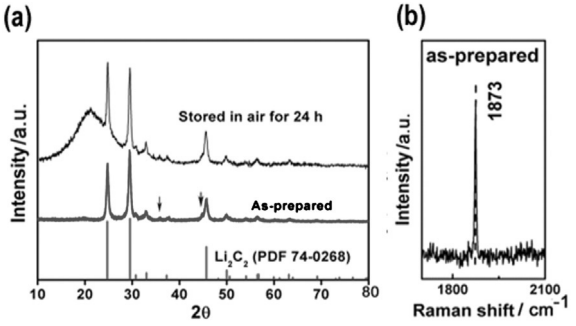

Figure 2. XRD patterns of the as-prepared and air-exposed Li_2C_2 (a) and Raman spectrum for the as-prepared Li_2C_2 (b).

for symmetrical stretching vibration of the C≡C bond appears at 1873 cm^{-1}, consistent with the results reported by Nylén et al.[18]

Figure 3 a shows the charge/discharge profiles of a Li_2C_2 cell between 2.0 and 4.6 V versus Li^+/Li. In the first cycle, the main charge process starts at approximately 4.3 V and ends at 4.6 V, consistent with the DFT predictions. The main discharge process is between 2.0 and 2.1 V. The discharge capacity of the cell reaches 700 mA h g^{-1} above 2.0 V. As the capacity of carbon black is only approximately 53 mA h g^{-1} under the same cycling conditions (Supporting Information, Figure S1), the actual capacity contribution of Li_2C_2 is 679 mA h g^{-1}, much higher than any other known inorganic cathode materials for lithium ion batteries. The possibility that electrolyte decomposition contributes significantly to the capacity of the cell can be excluded (Figure 3 a) because the specific capacity of the (CB + PTFE) electrode is very low in comparison with that of the (Li_2C_2 + CB + PTFE) electrode (53 mA h g^{-1} vs. 700 mA h g^{-1}) under the same cycling condition. The charge and discharge profiles become much steeper in the subsequent cycles than in the first cycle, and the capacity decreases to 300 and 180 mA h g^{-1} after two and five cycles, respectively. The capacity is stabilized at approximately 140 mA h g^{-1} after 10 cycles (Figure 3 b). This means that the C2 (C≡C) structure acts as the electron donor and acceptor in the Li_2C_2 material. These results suggest that some simple compounds can be used as high-capacity cathode materials of lithium ion batteries.

A potential gap of around 2.5 V appears in the potential profile of the first cycle of Li_2C_2. The ohmic resistance, charge transfer resistance, and diffusion resistance of the cell are three dynamic factors for the overpotential (ΔV). The relationship between ΔV and the current i can provide a clue to find out the main reasons for the dynamic overpotential.[19,20] ΔV is the difference between the potential at a certain current i and the equilibrium potential at that current. Figure 3 c shows that the equilibrium potential (25 % of the lithium is extracted) is 3.67 V according to the GITT profile. Figure 3 d further shows that ΔV is linearly dependent on lg(i). This means that charge transfer is the rate-controlling step during lithium extraction,[19,20] consistent with the large band gap (3.2 eV) and low electronic conductivity of Li_2C_2 obtained with DFT calculations (Figure 1 b). This is very similar to the situation of the lithium–air batteries, in which

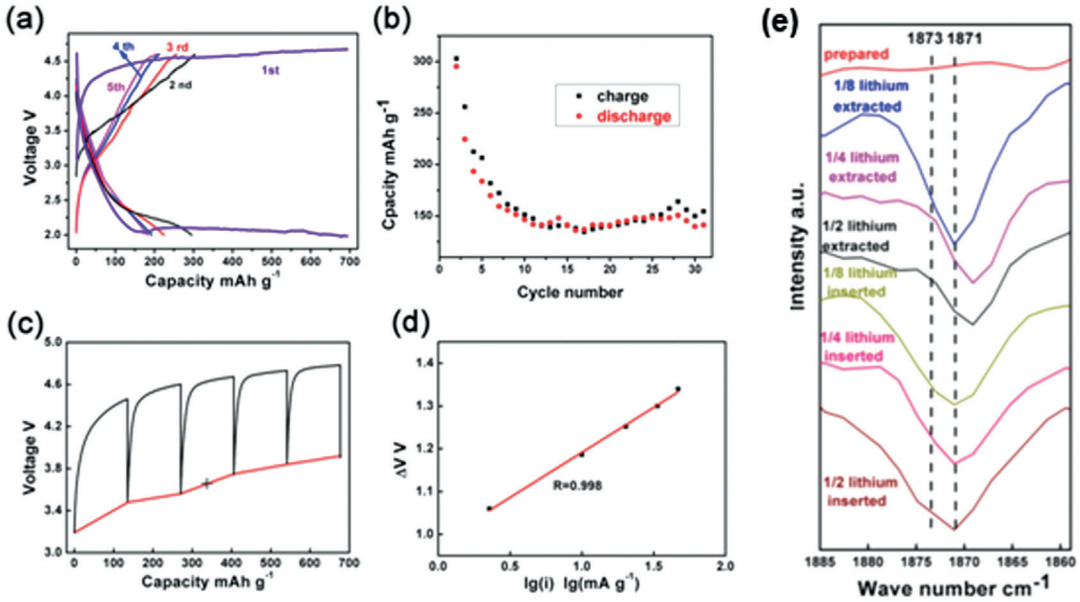

Figure 3. Charge/discharge curves (a) and cycle performance (b) of Li_2C_2, the GITT profile of Li_2C_2 during initial charge (c), linear fitting to the dependence of ΔV vs. lg(i) (d), and evolution of the FTIR spectrum of Li_2C_2 at various charge/discharge states (e).

the insulating nature and the difficulty of oxidation of Li_2O_2 and Li_2CO_3 leads to the large anodic overpotential.[21,22]

To evaluate lithium diffusion in Li_2C_2, first-principles molecular dynamics (FPMD) simulations were performed at temperatures ranging from 500 to 2000 K within a $3\times3\times2$ supercell ($Li_{72}C_{72}$) of the unit cell. The simulation time scale is 30 ps with a step length of 2 fs. It was observed that the ordering of the C≡C (bond length 1.257 Å; denoted as C2) dimers is very sensitive to the temperature. At a lower temperature (< 1200 K), the structure is ordered and the C2 dimers vibrate around their equilibrium positions. However, rotation and even migration are obviously observed for the C2 dimers as the simulation temperature increases to 1200 K. Therefore, a phase transition is expected to occur above 1200 K. In reality, a phase transition is observed at 800 K,[23] even though FPMD predicts that it will not occur below 1200 K, probably owing to the limited FPMD time in our simulation.

The diffusion coefficients (D) of the lithium ions were calculated by fitting the slope of mean square displacements (MSD) according to Equation (2). These diffusion coeffi-

$$D_{\mathrm{Li}} = \frac{1}{N}\lim_{t\to\infty}\frac{1}{6t}\left\langle\sum_i\left|\delta\vec{r}(t)\right|^2\right\rangle \qquad (2)$$

cients below 1200 K are used to acquire the activation energy (E_a) for lithium ions based on the Arrhenius equation. According to this, the activation energy for lithium ion diffusion in Li_2C_2 is calculated to be 0.50 eV (Figure 4a). This is a rather high energy barrier for ion diffusion. The divergence of the diffusion coefficients is probably due to the limited simulation time scale and the sensitivity of the structure to the temperature.

The low lithium diffusion coeffecient of Li_2C_2 is likely another reason for its poor charge transfer and large overpotential. However, the low electric conductivity may not prevent Li_2C_2 from becoming a promising high capacity cathode material for lithium ion batteries. A similar case is $LiFePO_4$ which was discovered in 1997,[24,25] but failed to be commercially applied until 1999 when Armand and coworkers[26] proposed to coat it with carbon, as well as to reduce its particle size.

Further analysis of the lithium trajectories from the FPMD simulations (at 1000 K) indicated that lithium diffusion in Li_2C_2 is three-dimensional, including five typical hops (Figure 4b). Paths 1 and 2 are hops perpendicular to the plane of C2 dimers, while paths 3, 4, and 5 are for migrations parallel to the plane of C2 dimers. Lithium migration along Path 1 requires the lowest energy. Two kinds of migration trajectories are detected along Path 1 during the FPMD simulations. One is a linear pathway (denoted as A), while the other is a curved pathway (denoted as B; Figure S2). However, the difference of the hopping energy barriers for these two trajectories (0.290 vs. 0.295 eV; Figure 4c) is negligible, according to the CI-NEB calculations. A longer diffusion length and a higher energy barrier (0.670 eV) are required for the other type of lithium hops (path 2; Figure 4d). The energy barriers for the migrations parallel to the plane of C2 dimers (paths 3, 4, and 5) are 0.456, 0.583, and 1.150 eV, respectively (Figure 4e to g). Clearly, the activation energy of 0.50 eV obtained from the Arrhenius fitting (Figure 4a) represents an average effect of various types of the lithium hops.

Structures of $Li_{53}C_{54}$ and $Li_{52}C_{54}$ were constructed by removing one and two lithium atoms from the $3\times3\times3$ supercell ($Li_{54}C_{54}$) of the primitive cell, respectively. These structures were relaxed to their equilibrium states on the basis of the first principles calculations. The simulations show that the C≡C dimers in Li_xC_2 ($0<x<2$) can easily rotate; chains with four C atoms (C4, C≡C···C≡C) are detected in many cases. For the former case (1/54 lithium ions removed), simulation at 700 K for 12 ps demonstrates the presence of C4 chains near the lithium vacancy (Figure 4h). For the latter

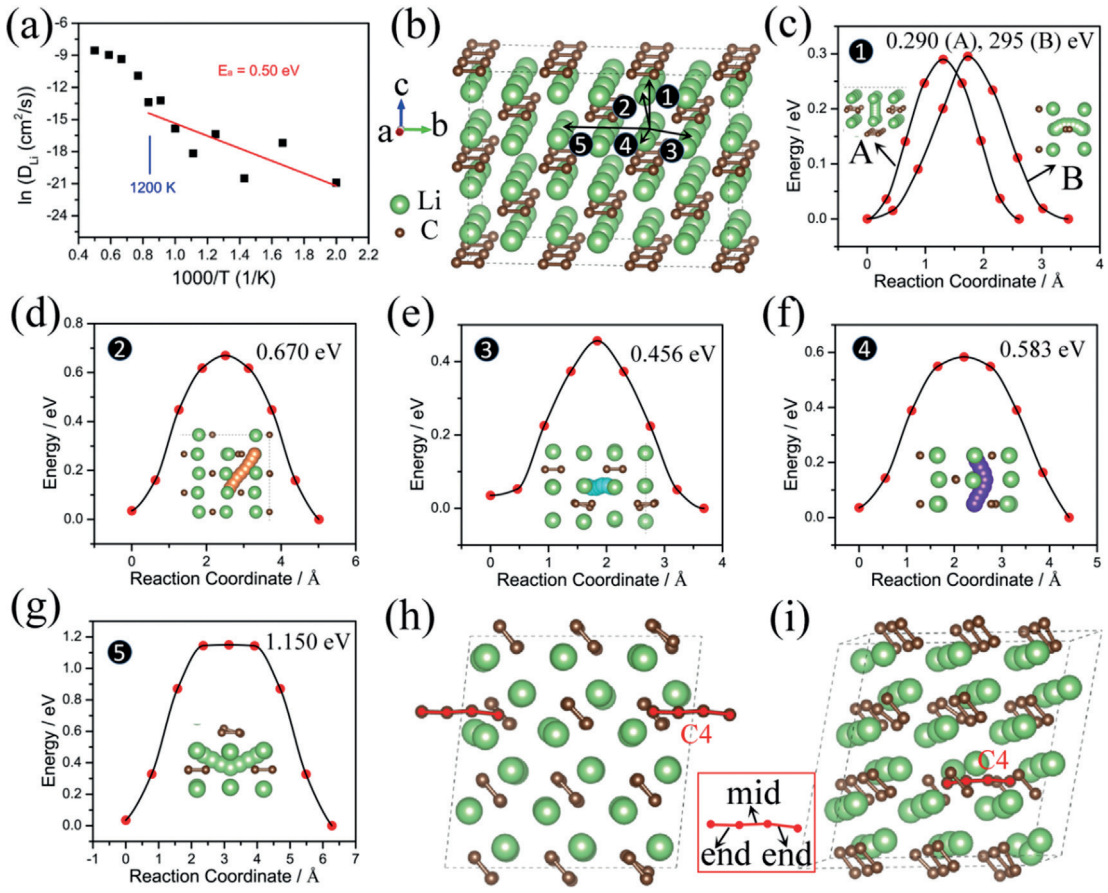

Figure 4. Arrhenius plot of Li diffusion in Li_2C_2 (a); the five possible hops between two neighboring Li sites (denoted with arrows) for the FPMD simulation (b), and the migration energy barrier of each calculated by CI-NEB method (c–g). The insets are the corresponding migration pathways. The relaxed structure of h) $Li_{53}C_54$ after FPMD simulation at 700 K), and i) $Li_{52}C_{54}$ after FPMD simulation at 300 K. The simulation time scale is 12 ps. The inset in (i) displays a C4 chain composed of two C2 bonds at both ends and one bond that connects these C2 bonds (denoted as "end" and "mid", respectively).

structure (2/54 lithium ions removed), the energy of the system gradually decreases with the increasing distance between the two vacancies (Figure S3). That is, the two vacancies tend to get farther away from each other so that they cannot interfere with each other.

The ground state was adopted for the FPMD simulation of $Li_{52}C_{54}$. Simulation at 300 K for 12 ps shows the existence of C4 chains as well (Figure 4i). With increasing temperature, the C4 chain can be formed in a shorter time, 2 ps at 500 and 700 K (Figure S4). The C4 chains are formed mainly in two ways. One way is a direct formation by the rotation and approaching of two adjacent C≡C dimers near the lithium vacancy. The other route is by, first, the migration of the nearby lithium ions towards the lithium vacancy, and then the formation of the C4 chain near the vacancy generated by the migrated lithium ions.

These results suggest that the C4 chain tends to be formed in delithiated Li_xC_2 ($0 < x < 2$). Table S2 shows that when 2/54 Li ions are removed, the length of each "end" bond of a C4 chain (inset of Figure 4i) decreases from 1.257 Å in pristine Li_2C_2 to 1.255 Å. That is, the end bond appears to remain a C≡C triple bond; lithium removal does not damage the structure of Li_2C_2 significantly. However, the length of the middle bond is approximately 1.37 Å, somewhere between that of a single bond and a double bond.[15] These indicate that the connection of the two C≡C bonds is strong and hard to be opened. Therefore, the charge profile of the second cycle is much different from that of the first cycle, and the capacity decreases quickly with cycling (Figure 3a). However the stabilized capacity of 140 mA h g^{-1} (Figure 3b) indicates that the structure does not collapse completely until half of the lithium in Li_2C_2 is extracted. As a result, Li_2C_2 is still a promising cathode material.

The structures with C4 chains display lower energy (ca. 1.13–4.74 eV) than that of the pristine Li_2C_2 (Figure S5). This will result in lower delithiation potentials than that expected for pristine Li_2C_2 (4.2 V), as discussed above. Furthermore, the presence of the C4 chain also affects the electronic structure of Li_2C_2. The delithiated Li_2C_2 would become metallic if the C4 chain was not formed. However, because the C4 chain thermodynamically prefers to be formed (Figure S5), its formation makes the Fermi level rise and opens a gap between the valence and conduction bands (Figure S6). Moreover, the band gap is narrower than that of the perfect Li_2C_2 before delithiation.

The evolution of the C≡C bond during lithium insertion and extraction was characterized with FTIR spectroscopy (Figure 3e). Theoretically, the symmetrical stretching of the

C≡C bond is Raman active but infrared inactive in a perfect Li_2C_2 crystal.[18] However, if lithium defects (such as vacancy) appear, or the C4 chains form after lithium extraction, then the C≡C stretching can become infrared active. The central position of the Raman peak for symmetrical stretching vibration of the C≡C bond appears at 1873 cm^{-1} (Figure 2b) though no infrared absorption peaks can be observed around it for the as-prepared material (Figure 3e). An infrared peak appears at 1871 cm^{-1} when 12.5% lithium is extracted from Li_2C_2, consistent with the above analysis. As more (50%) lithium ions are extracted, the peak position shifts to 1868 cm^{-1}. When the lithium ions are re-inserted into $Li_{2-x}C_2$, the absorption peak goes back to 1871 cm^{-1} in the FTIR spectrum. These spectroscopic results are in agreement with the slight changes of the length of the C≡C bond in a C4 chain (1.257 vs. 1.255 Å). Therefore, the structural variation of Li_2C_2 is negligible in lattice parameters and the delithiation-induced C4 structure is very stable.

In conclusion, Li_2C_2 was synthesized by a solid state reaction and used as a high-capacity cathode material for lithium ion batteries. Electrochemical performance evaluation indicates that at least half of the lithium in Li_2C_2 can be reversibly extracted and inserted. A reversible capacity of 700 mA h g^{-1} can be obtained in the initial cycle, and the capacity is stabilized at 140 mAh g^{-1}. In this material, the C2 acts as both the electron donor and electron acceptor. The potential gap between charge/discharge was found to be a dynamic and thermodynamic overpotential. First-principles based DFT and FPMD calculations indicate that low electronic conductivity and lithium diffusion in Li_2C_2 is responsible for the dynamic overpotential. Calculations further show that delithiation leads to the rotation and migration of the C≡C bonds, and the formation of the C4 chains (C≡C···C≡C). Generation of a strong middle bond that connects the two C≡C bonds damages the symmetry of Li_2C_2 and leads to the activation of C≡C stretching in the FTIR spectrum. However, the negligible position shifting of the C≡C stretching in the FTIR spectrum during charge/discharge demonstrates the structural stability of Li_2C_2 during delithiation and relithiation. Therefore, although the electrochemical performance of Li_2C_2 does not meet the requirement of current high energy-density lithium ion batteries, its performance can be improved by surface modification (coated with conducting species), reduction of the particle size, and elemental substitution. Besides applications as a cathode material, Li_2C_2 can also be used as cathode additives for lithium ion batteries using silicon anodes. Considering the large family of the alkali and alkaline earth metal carbides, and the cost-effective and environmentally friendly features of the carbides, our findings also provide insight into the development of high-performance electrode materials for sodium ion batteries and secondary magnesium batteries.

Acknowledgements

This work was financially supported by the National 973 Program of China (No. 2015CB251100), the National Natural Science Foundation of China (NSFC, No. 51372268 and No. 11234013) and the German Research Foundation (SPP 1473-SO 1075/1-2).

Keywords: density functional theory · high capacity · Li_2C_2 · lithium ion battery

How to cite: *Angew. Chem. Int. Ed.* **2016**, *55*, 644–648
Angew. Chem. **2016**, *128*, 654–658

[1] A. Boulineau, L. Simonin, J. F. Colin, C. Bourbon, S. Patoux, *Nano Lett.* **2013**, *13*, 3857–3863.
[2] L. Simonin, J. F. Colin, V. Ranieri, E. Canévet, J.-F. Martin, C. Bourbon, C. Baehtz, P. Strobel, L. Daniel, S. Patoux, *J. Mater. Chem.* **2012**, *22*, 11316–11322.
[3] M. M. Thackeray, S.-H. Kang, C. S. Johnson, J. T. Vaughey, R. Benedek, S. A. Hackney, *J. Mater. Chem.* **2007**, *17*, 3112–3125.
[4] C. Fu, G. Li, D. Luo, J. Zheng, L. Li, *J. Mater. Chem. A* **2014**, *2*, 1471–1483.
[5] H. Kim, D.-H. Seo, G. Yoon, W. A. Goddard, Y. S. Lee, W.-S. Yoon, K. Kang, *J. Phys. Chem. Lett.* **2014**, *5*, 3086–3092.
[6] H. Zhang, Q. Deng, A. Zhou, X. Liu, J. Li, *J. Mater. Chem. A* **2014**, *2*, 5696–5702.
[7] L. Shen, Z. Wang, L. Chen, *Chem. Eur. J.* **2014**, *20*, 12559–12562.
[8] Z. Song, H. Zhou, *Energy Environ. Sci.* **2013**, *6*, 2280–2301.
[9] F. Chevallier, F. Poli, B. Montigny, M. Letellier, *Carbon* **2013**, *61*, 140–153.
[10] T. L. Chwang, R. West, *J. Am. Chem. Soc.* **1973**, *95–10*, 3324–3330.
[11] L. A. Shimp, J. A. Morrison, J. A. Gurak, J. W. Chinn, R. J. Lagow, *J. Am. Chem. Soc.* **1981**, *103*, 5951–5953.
[12] S. Konar, U. Häusserman, G. Svensson, *Chem. Mater.* **2015**, *27*, 2566–2575.
[13] *Gmelins Handbuch der Anorganischen Chemie*, 8th ed., Berlin, **1960**.
[14] R. Juza, V. Wehle, *Naturwissenschaften* **1965**, *52*, 537–537.
[15] P. L. Carl, *The nature of the chemical bond*, 3 ed., Cornell University Press, Ithaca, **1960**.
[16] R. Schmitz, R. A. Müller, R. W. Schmitz, C. Schreiner, M. Kunze, A. Lex-Balducci, S. Passerini, M. Winter, *J. Power Sources* **2013**, *233*, 110–114.
[17] N. Tian, C. Hua, Z. Wang, L. Chen, *J. Mater. Chem. A* **2015**, *3*, 14173–14177.
[18] J. Nylén, S. Konar, P. Lazor, D. Benson, U. Häussermann, *J. Chem. Phys.* **2012**, *137*, 224507–1–224507–8.
[19] W. Dreyer, J. Jamnik, C. Guhlke, R. Huth, J. Moskon, M. Gaberscek, *Nat. Mater.* **2010**, *9*, 448–453.
[20] B. Zhang, Z. Wang, H. Li, X. Huang, *J. Power Sources* **2011**, *196*, 6992–6996.
[21] T. Ogasawara, A. Débart, M. Holzapfel, K. P. Nova, P. G. Bruce, *J. Am. Chem. Soc.* **2006**, *128*, 1390–1393.
[22] S. H. Oh, L. F. Nazar, *Adv. Energy Mater.* **2012**, *2*, 903–910.
[23] U. Ruschewitz, R. Pöttgen, *Z. Anorg. Allg. Chem.* **1999**, *625*, 1599–1603.
[24] A. K. Padhi, K. S. Nanjundaswamy, J. B. Goodenough, *J. Electrochem. Soc.* **1997**, *144*, 1188–1194.
[25] A. K. Padhi, K. S. Nanjundaswamy, C. Masquelier, S. Okada, J. B. Goodenough, *J. Electrochem. Soc.* **1997**, *144*, 1609–1613.
[26] N. Ravet, J. B. Goodenough, S. Besner, M. Simoneau, P. Hovington, M. Armand, *The Electrochemical Society and The Electrochemical Society of Japan Meeting Abstracts* **1999**, *127*, 99–2.

Received: September 28, 2015
Revised: October 24, 2015
Published online: November 26, 2015

